Applied Science and Innovative Research
ISSN 2474-4972 (Print) ISSN 2474-4980 (Online)
Vol. 4, No. 4, 2020
www.scholink.org/ojs/index.php/asir

Original Paper

Humidity Degradation Study of Mesa-type Avalanche Photodiodes under Harsh Environmental Stresses

Jack Jia-Sheng Huang[1,2*], H.S. Chang[2], Emin Chou[2], Yu-Heng Jan[2,1] & Jin-Wei Shi[3]

[1] Source Photonics, 8521 Fallbrook Avenue, Suite 200, West Hills, CA 91304, USA

[2] Source Photonics, No.46, Park Avenue 2nd Rd., Science Park, Hsinchu, Taiwan

[3] Department of Electrical Engineering, National Central University, Zhongli, Taiwan

[*] Correspondence: Jack J.S. Huang, E-mail: jack.huang@sourcephotonics.com

Received: September 8, 2020 Accepted: September 30, 2020 Online Published: October 9, 2020

doi:10.22158/asir.v4n4p9 URL: http://dx.doi.org/10.22158/asir.v4n4p9

Abstract

Avalanche photodiode is a widely used receiver component due to its high sensitivity and low noise performance. For many applications, the APD chips are required to maintain stable performance against harsh environmental stresses such as high heat and humidity. In this paper, we study the APD moisture degradation behavior under the harsh environment of high humidity (60-75%), high temperature (85℃), and high bias (-32 V). We present empirical acceleration factor form functions of temperature and humidity based on experimental data and provide quantitative analysis on the humidity dependence. The humidity coefficient of the mesa-type APD from exponential fit is estimated to be -0.00137.

Keywords

Avalanche photodiodes, photodiodes, reliability, humidity dependence, dark current, harsh environmental stress, electrochemical oxidation

1. Introduction

Avalanche photodiode (APD) provides versatile performance advantages for photoreceivers including high sensitivity, high signal-to-noise ratio, and low dark current (Campbell, 2016; Nada et al., 2015; Huang et al., 2017; Chen et al., 2018; Neitzert et al., 1997; Huang et al., 2020). Because of those technological benefits, the APDs are widely deployed in commercial and military applications such as military, passive optical network (PON), telecommunication, and wireless (as illustrated in Figure 1). Recently, APD reliability, under harsh environmental stresses such as high heat and humidity, has drawn great interest to meet up the cost and performance requirements. A robust APD needs to

maintain stable performance under harsh environments such as heat, moisture, and radiation (Huang et al., 2017; Huang et al., 2018).

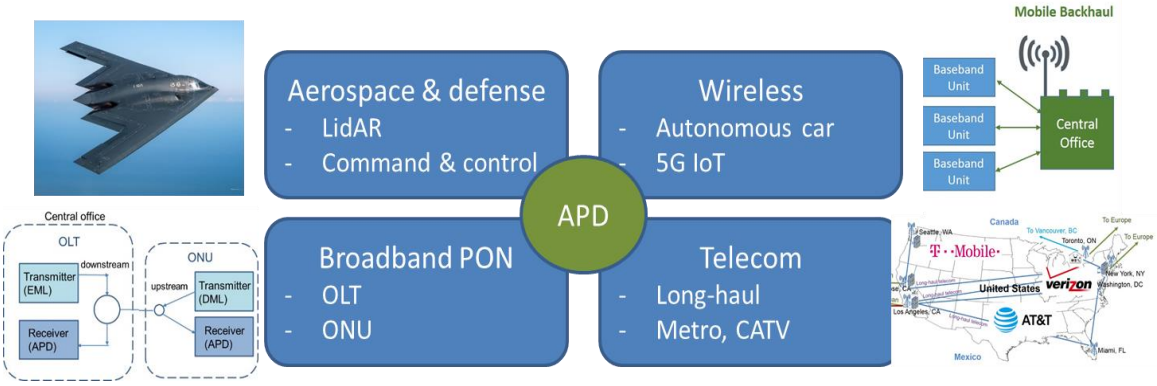

Figure 1. Illustration of APD Applications in the Areas of Military, PON, Telecommunication, and Wireless

Most of the APD reliability studies were focused on aging behavior against heat (Huang et al., 2018; Ishimura et al., 2007; Kim et al., 2001; Takeshita et al., 2006; Watanabe et al., 1996; Smith et al., 2009). Very few literature was reported on the combined effect of moisture and heat. Knowledge of the APD degradation behavior against moisture is becoming increasingly important for low cost non-hermetic applications. Although some empirical non-hermetic reliability data have been presented, fundamental understanding of the failure mechanisms under non-hermetic environment still remains relatively scarce compared to the classical degradation case under heat (Comizzoli et al., 2001; Osenbach et al., 1996).

In this paper, we study the effect of temperature and humidity on the degradation of mesa-type APD. We show the humidity dependence of the mesa-type APD based on the empirical formula and discuss the implication of humidity sensitivity.

2. Experimental

Figure 2 shows the schematics of a mesa-type APD used in this reliability study. The APD device was based on mesa structure with coplanar P- and N-metal contacts to enhance the speed and reduce the series resistance (Huang et al., 2017). The top P-mesa consisted of InGaAs contact layer and InP window (Huang et al., 2016). The p-InGaAs contact layer was covered by the p-metal to form Ohmic contact and connected to the bondpad by a p-metal ring that surrounded the circular anti-reflective (AR) window. The active region consisted of the InGaAs absorption (1.2 μm), nanoscale InAlAs charge control (50 nm), and InAlAs multiplication (200 nm) layers. Such active structure was also called separate absorption, charge, and multiplication (SACM). Electron carrier was utilized for multiplication of the mesa-type APD (Huang et al., 2018). The bottom N-mesa consisted of the N-InP buffer and

contact layers, grown on a semi-insulating (S.I.) InP substrate. The N-mesa was covered by the n-metal contact that was connected to the n-metal bondpad. For the passivation dielectrics, a thick polyimide (~2-3 μm) was used to reduce the capacitance, covered by a thin SiO_2 coating (320 nm) to enhance surface passivation.

(a)

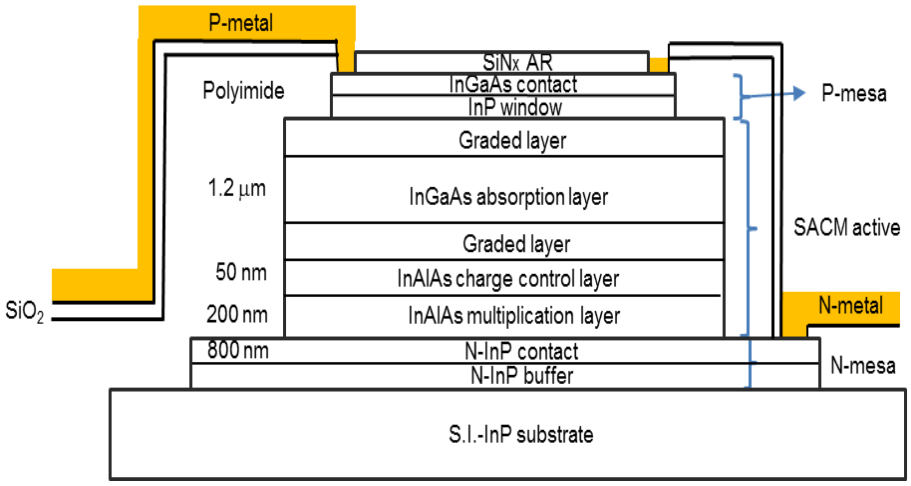

(b)

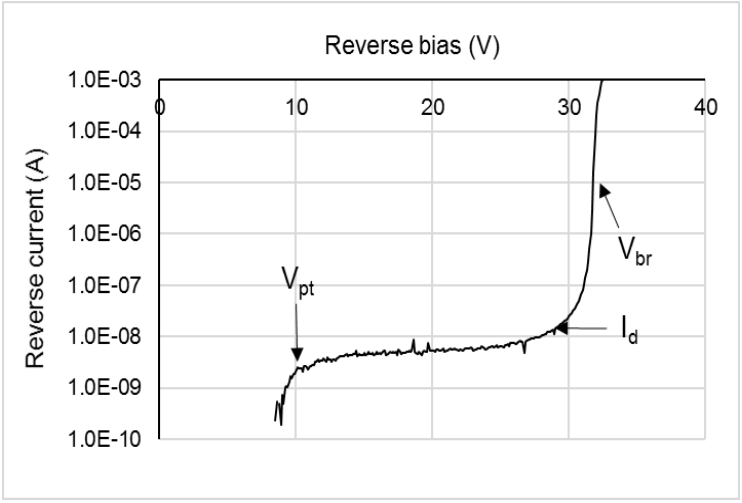

Figure 2. (a) Schematics of the Mesa-type SACM APD Structure Used in the Harsh Environmental Study. (b) The Reverse IV Curve of the Mesa-type APD Measured at 25°C. The Horizontal Axis Shows the Absolute Value of the Reverse Voltage

Figure 2(b) shows the reverse current-voltage (IV) curve of the mesa-type SACM APD. The IV curve shows two transitions where the slopes of the curve change drastically. The first transition at 10 V corresponds to the punch-through voltage at which electric field depletes both the InAlAs multiplication and *i*-InGaAs absorption layers (Huang et al., 2017). The punch-through voltage related to the absorption layer is denoted as V_{pt}. The second transition represents the avalanche breakdown

voltage (V_{br}) that is typically determined by the InAlAs multiplication layer. The V_{br} measured at 10 μA on the IV curve is about 32 V. The dark current (I_d) taken by the reverse current at $0.9V_{br}$ is estimated to be about 12 nA at 25°C.

For the harsh environmental stress experiment, the APD chips were mounted on transistor outline (TO) headers. Gold wire was bonded to connect the p-metal contact of the APD to the electrical lead of the TO header. The APD samples were placed into sockets of the circuit board, and the circuit board was inserted in the chamber. Electrical current-voltage (IV) test was measured before and after each stress. The moisture containing ambient (MCA) chamber was set at various temperatures and relative humidities (RH). All the APD devices were biased at -32 V near its breakdown voltage (V_{br}).

To study the APD degradation behavior under humidity and heat, three groups of samples were tested for different stress conditions. Group-A was tested under the MCA condition of 25°C/75% RH. Group-B was tested under the MCA condition of 85°C/60% RH. Group-C was tested under the condition of 85°C/0% RH where the TO samples were sealed to simulate 0% RH. The IV was monitored at 0, 160, 500, and 1000 hours of MCA stress. The device lifetime was defined as the time to reach 10 times of the initial dark current.

Following the 1000-hour stress test, the most severely degraded devices were examined by optical microscopy (OM) and scanning electron microscopy (SEM) to identify the failure site.

3. Results and Discussions

Figure 3 shows the distributions of relative dark current changes of the mesa-type APD devices subjected to the three different stress conditions (Group-A, Group-B, and Group-C). The relative dark current change was taken by the ratio of the dark current after 1000-hour stress versus the initial dark current. Group-A (25°C/75% RH) showed the most pronounced dark current change despite of no temperature acceleration. This suggested that the effect of humidity was more dominant than the effect of temperature. Group-B (85°C/60% RH) showed the second most dark current change. Group-C (85°C/0% RH) showed the least dark current change, indicating that the temperature acceleration was less influential than the humidity acceleration. Table 1 summarizes the median dark current changes of the three stress groups. The median changes of dark current were 13.8, 8.0, and 1.0 for Group-A, Group-B, and Group-C, respectively.

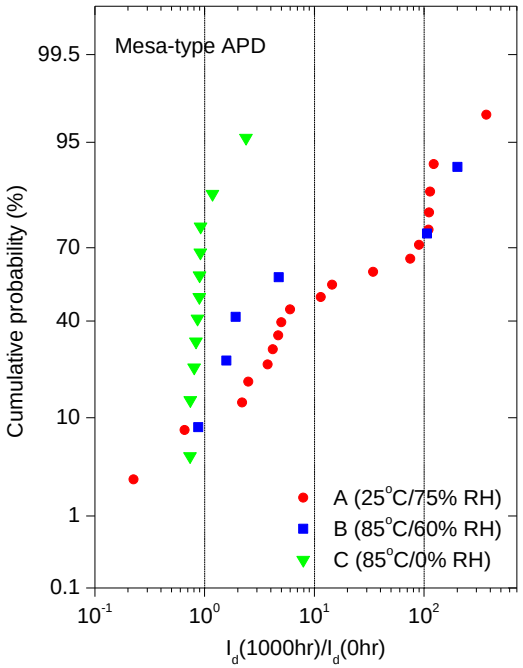

Figure 3. Relative Dark Current Change Distributions of the Mesa-type APD Devices under Three Stress Conditions (25°C/75% RH, 85°C/60% RH, and 85°C/0% RH)

Table 1. Summary of Humidity/Temperature Stress Test Results of Mesa-type APD Devices

	Group-A 25°C/75% RH	Group-B 85°C/60% RH	Group-C 85°C/0% RH
Environmental stress	Harsh humidity	Humidity and temperature	Only temperature
Median dark current change ratio, I_d(1000hr)/I_d(0hr)	13.8	8.0	1.0
Stress results	Effect of humidity was dominant	Effect of temperature was less significant than humidity	Effect of temperature was less significant than humidity

Figure 4(a) and (b) show the top-view optical and SEM images of the mesa-type APD device after the moisture environmental test. Optical inspection showed that the circled region of the p-metal bridge was vulnerable to moisture-induced damage. On the sides of the p-metal bridge near the p-metal pad, there was only passivation of thin SiO_2 and polyimide, but no p-metal on the surface. In the moisture ambient, water penetration was more likely to initiate from the sides where the p-metal was absent. After the incubation phase, the water gradually propagated inwards to cause further damage.

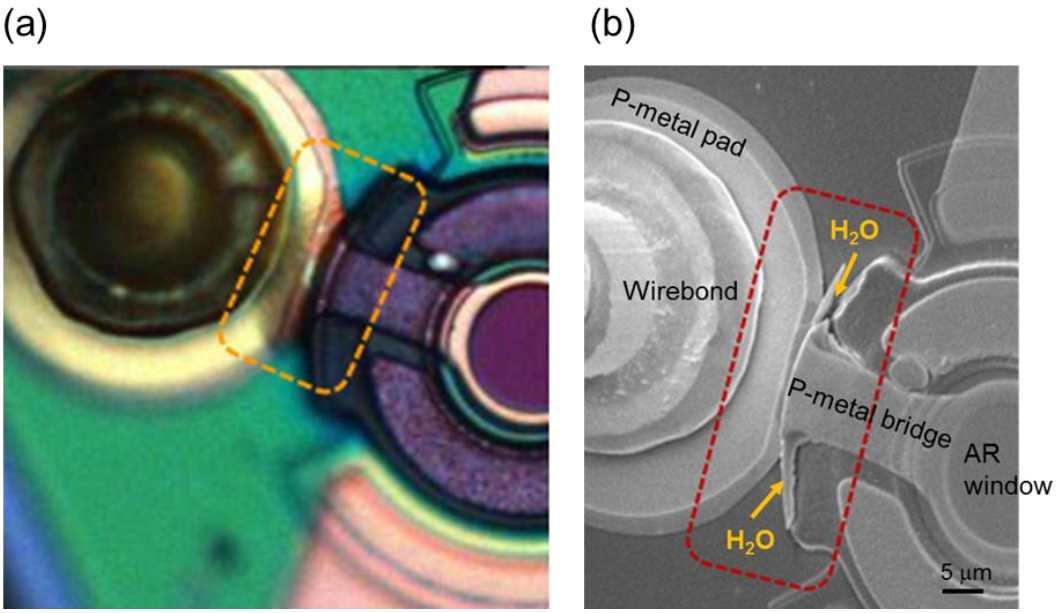

Figure 4. Top-view (a) Optical and (b) SEM Image of the Mesa-type APD Device after Moisture Degradation. Examination of the Most Severely Damaged Device from Group-A showed Damage on the Sides of the p-metal Bridge

3.1 Moisture Degradation Model

As reported in our previous study, the moisture degradation of the mesa-type APD can be explained by our model summarized below (Huang et al., 2020).

a) When the mesa-type APD device was subjected to harsh environmental stresses (25-85 °C, 60-75% RH, -32 V), the applied voltage generated relatively high electric field across the passivation layer (Huang et al., 2017). The high electric field was particularly pronounced at the edge of polyimide where the layer was thinned down and exposed to field gradient near the wirebond area.

b) The high electric field caused leakage current to flow through the passivation layer, assisted by surface leakage. The combination of current flow and moisture-containing ambient led to electrochemical oxidation (Chakrabarti et al., 2002).

c) During the electrochemical oxidation process, moisture reacted with InP and resulted in nucleation of indium phosphate ($InPO_4$) compound.

d) As the compound grew over time, the $InPO_4$ compound formed high stress regions that caused bulging in the polyimide and metal bridge. Typically, the moisture degradation incurred an increase in dark current as shown in Figure 3. For the severe case, the bulging may also rupture the metal bridge to cause open failure.

3.2 Device Lifetime and Acceleration Factor

For the classical aging test that involves only temperature, the device lifetime (t_f) typically follows Black's equation where E_a is the activation energy, k is the Boltzmann's constant, and T is the absolute temperature in K (Huang et al., 2020; Huang et al., 2017).

$$t_f \propto \exp(E_a/kT) \quad (1)$$

In cases involving harsh environmental stresses, the device lifetime includes the acceleration factors of (1) temperature, (2) moisture, and (3) applied voltage. The humidity and voltage form functions are not well defined by theory. Here, we adopt the functions in the Osenbach model as depicted in Equation (2) where A is the humidity coefficient and B is the bias coefficient (Osenbach et al., 1996). The exponential dependence on RH has been observed for various insulator surfaces (Comizzoli et al., 2001).

$$t_f \propto \exp(E_a/kT) \exp[A(RH)^n] \exp(BV) \quad (2)$$

Since the effect of moisture was more dominant, we conducted detailed quantitative analysis on the humidity acceleration. Figure 5(a) shows the natural logarithm of the median lifetime versus relative humidity (% RH) of the mesa-type APD devices based on linear fit. The line shows the best fit of least squares of the data. For Group-A, we used the activation energy of 0.42 eV to extrapolate the lifetime at 85°C (Osenbach et al., 1996). The exponential humidity coefficient for the linear fit (where n=1) is -0.0962 with a R^2 correlation factor of 0.900. Figure 5(b) is a plot of the natural logarithm of the median lifetime versus relative humidity squared two (% RH^2) of the same mesa-type APD samples. The exponential humidity coefficient for n=2 is -0.00137 with a R^2 correlation factor of 0.994. Comparing the fitting of n=1 and n=2, we conclude that the square fit using n=2 is statistically better. Based on the analysis, we take the humidity dependence for the mesa-type APD devices to be the form expressed in Equation (3).

$$t_f \propto \exp(E_a/kT) \exp[A(RH)^2] \exp(BV) \quad (3)$$

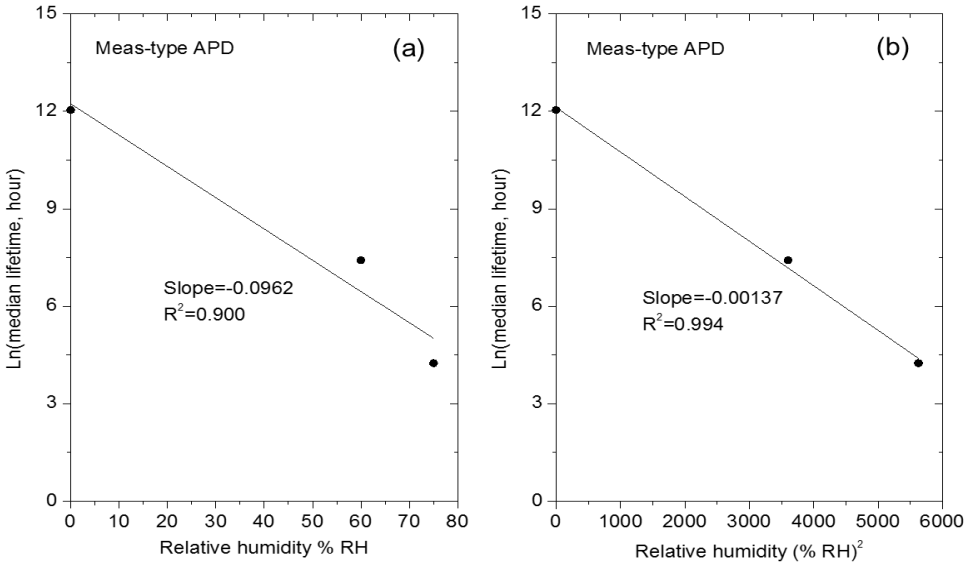

Figure 5. (a) Plot of Median Lifetime versus Relative Humidity Using Linear Model (n=1) and (b) Plot of Median Lifetime versus Relative Humidity Squared Two Where n=2 in Equation (2). Both Linear and Squared Fits are Applied to the Same Experimental Data from Group-A, Group-B, and Group-C

We note that the humidity coefficient value of 0.00137 for the mesa-type APD is greater that the value of 0.00046 reported in the planar InP p-type/intrinsic/n-type (PIN) photodiodes (Osenbach et al., 1996). The higher empirical value of humidity coefficient indicates higher sensitivity to the environmental moisture. By taking the square root of the ratio of humidity coefficient of mesa-type versus planar-type APD, the humidity sensitivity of the mesa-type is estimated to be higher than that of the planar-type by a factor of 1.7. This is expected because the mesa-type structure is likely to generate more weak spots resulting from surface state, geometrical non-uniformity, and topography (Huang et al., 2016; Huang et al., 2020).

4. Conclusion

We have studied the moisture-induced reliability degradation of mesa-type APD under harsh environmental stress of high humidity, high temperature, and high bias. We characterized the dark current change distributions of the three different stress conditions (25°C/75% RH/-32 V, 85°C/60% RH/-32 V, and 85°C/0% RH/-32 V). The data suggested that humidity effect was more dominant than temperature and bias.

We also observed that the moisture-induced damage typically occurred on the sides of the p-metal bridge due to the topography of APD mesa structure. The humidity degradation was manifested by the increase in dark current. In the severe case, open failure was also likely to occur due to the rupture of p-metal bridge from the formation of $InPO_4$ compound underneath.

The quantitative analysis of the humidity dependence showed that the degradation of the mesa-type APD followed squared-two dependence of humidity (% RH^2). The humidity coefficient was determined to be -0.00137. The higher value of humidity coefficient indicated higher sensitivity to the environmental moisture than that of the planar-type APD, by a factor of 1.7.

Acknowledgments

The authors would like to thank C.J. Ni (Source Photonics, Taiwan) for wafer processing and Shannon Huang (UCLA, USA) for proofreading.

References

Campbell, J. C. (2016). Recent advances in avalanche photodiodes. *J. Lightwave Tech., 34*(2), 278-285. https://doi.org/10.1109/JLT.2015.2453092

Chakrabarti, U. K., Comizzoli, R. B., Osenbach, J. W., & Theis, C. (2002). *Nonhermetic APD, US Patent 6,489,659.*

Chen, Y. H., Wun, J. M., Wu, S. L., Chao, R. L., Huang, J. S., Jan, Y. H., … Shi, J.-W. (2018). Top-illuminated $In_{0.52}Al_{0.48}As$-based avalanche photodiode with dual charge layers for high-speed and low dark current performances. *J. Selected Topics Quantum Electronics*, *24*(2), 3800208. https://doi.org/10.1109/JSTQE.2017.2731938

Comizzoli, R. B., Osenbach, J. W., Crane, G. R., Peins, G. A., Siconolfi, D. J., Lorimor, O. G., & Chang, C.-C. (2001). Failure mechanism of avalanche photodiodes in the presence of water vapor. *J. Lightwave Tech., 19*(2), 252-265. https://doi.org/10.1109/50.917897

Huang, J. S., & Jan, Y. H. (2017). *Environmental Engineering of Photonic and Electronic Reliabilities: from Technology and Energy Efficiency Perspectives*. Scholars' Press, Saarbrücken, Germany.

Huang, J. S., Chang, H. S., & Jan, Y. H. (2017). Reliability challenges of nanoscale avalanche photodiodes. *Open Access J. Photoenergy*, 0015. https://doi.org/10.15406/mojsp.2017.01.00015

Huang, J. S., Chang, H. S., Chou, E., Jan, Y. H., & Shi, J.-W. (2020). Novel failure mechanism of nanoscale mesa-type avalanche photodiodes under harsh environmental stresses. *IET Nanodielectrics*, in review.

Huang, J. S., Chang, H. S., Jan, Y. H., Chen, H. S., Ni, C. J., & Chou, E. (2017). Temperature dependence study of mesa-type InGaAs/InAlAs avalanche photodiode characteristics, *Adv. Optoelectronics*, *2084621*, 1-5. https://doi.org/10.1155/2017/2084621

Huang, J. S., Chang, H. S., Jan, Y. H., Chen, H. S., Ni, C. J., Chou, E., … Shi, J.-W. (2018). *Highly reliable, cost-effective and temperature-stable top-illuminated avalanche photodiode (APD) for 100G inter-datacenter ER4-Lite applications*. Photoptics, Funchal, Portugal.

Huang, J. S., Chang, H. S., Jan, Y. H., Ni, C. J., Lee, S. K, Chen, H. S., … Shi, J.-W. (2020). *Reliability challenges of nanoscale avalanche photodiodes for high-speed fiber-optic communications*. Book chapter for Recent developments and trends in optics, photonics and laser technologies: Insights from PHOTOPTICS 2018 (Springer, Germany, 2020), Editor Maria Raposo and Paulo A. Ribeiro, Chapter 7, 143-167. https://doi.org/10.1007/978-3-030-30113-2_7

Huang, J. S., Jan, Y. H., Chang, H. S., Ni, C. J., Chou, E., Lee, S. K., … Shi, J.-W. (2018). *Nanoscale III-V semiconductor photodetectors for high-speed optical communications*. Chapter 3. Two-dimensional materials for photodetector. Edited by P. Kumar Nayak, (Rijeka, Croatia, InTech Open), 49-73. https://doi.org/10.5772/intechopen.73054

Huang, J. S., Jan, Y. H., Chen, H. S., Chang, H. S., Ni, C. J., & Chou, E. (2016). Predictive reliability model of 10G/25G mesa-type avalanche photodiode degradation, *Appl. Phys. Res., 8*(3), 66-74. https://doi.org/10.5539/apr.v8n3p66

Ishimura, E., Yagyu, E., Nakaji, M., Ihara, S., Yoshiara, K., Aoyaji, T., … Ishikawa, T. (2007). Degradation mode analysis on highly reliable guardring-free planar InAlAs avalanche photodiode. *J. Lightwave Tech., 25*(12), 3686-3693. https://doi.org/10.1109/JLT.2007.909357

Kim, H. S., Choi, J. H., Bang, H. M., Jee, Y., Yun, S. W., Burm, J., … Choo, A. G. (2001). Dark current reduction in APD with BCB passivation. *Electron. Lett., 37*(7), 455-457. https://doi.org/10.1049/el:20010318

Nada, M., Yoshimatsu, T., Muramoto, Y., Yokoyama, H., & Matsuzaki, H. (2015). Design and Performance of High-Speed Avalanche Photodiodes for 100-Gb/s Systems and Beyond.

IEEE/OSA Journal of Lightwave Technology, *33*(5), 984-990. https://doi.org/10.1109/JLT.2014.2377034

Neitzert, H. C., Cappa, V., & Crovato, R. (1997). *Influence of the device geometry and inhomogeneity on the electrostatic discharge sensitivity of InGaAs/InP avalanche photodiode*. EOS/ESD Symposium (Santa Clara, CA).

Osenbach, J. W., & Evanosky, T. L. (1996). Temperature-humidity-bias-behavior and acceleration model for InP Planar PIN photodiodes. *J. Lightwave Tech.*, *14*(8), 1865-1881. https://doi.org/10.1109/50.532025

Smith, G. M., McIntosh, K. A., Donnely, J. P., Funk, J. E., Mahoney, L. J., & Verghese, S. (2009). Reliable InP-based Geiger-mode avalanche photodiode array. *Proceedings of SPIE*, *7320*, 1-10. https://doi.org/10.1117/12.819126

Takeshita, T., Hirota, Y., Ishibashi, T., Muramoto, Y., Ito, T., Tohmori, Y., & Ito, H. (2006). Degradation behavior of avalanche photodiodes with a mesa structure observed using a digital OBIC monitor. *IEEE Trans. Electron Devices*, *53*(7), 1567-1574. https://doi.org/10.1109/TED.2006.875820

Watanabe, I., Tsuji, M., Hayashi, M., Makita, K., & Taguchi, K. (1996). Reliability of mesa-structure InAlGaAs-InAlAs superlattice avalanche photodiodes. *IEEE Photonics Tech. Lett.*, *8*(6), 824-826. https://doi.org/10.1109/68.502107